Free-surface dynamics in the Ribbon Growth on Substrate (RGS) Process

Beckstein, P.; Galindo, V.; Gerbeth, G.;

Originally published:

February 2017

International Journal of Applied Electromagnetics and Mechanics 53(2017)51, 543-551

DOI: https://doi.org/10.3233/JAE-162237

Free-surface dynamics in the Ribbon Growth on Substrate (RGS) Process

Pascal Beckstein*, Vladimir Galindo, Gunter Gerbeth
Department of Magnetohydrodynamics, Institute of Fluid Dynamics, Helmholtz-Zentrum Dresden-Rossendorf, Dresden, Germany

Abstract. With the Ribbon Growth on Substrate (RGS) technology, a new crystallization technique is available that allows controlled high crystallization rate production of silicon wafers and advanced metal-silicide alloys. Compared to other casting methods, such as e.g. directional solidification, the RGS process allows better crystallization control, high volume manufacturing and high material yield due to its continuous, substrate-driven design. Insights from modelling the characteristic melt flow in the casting frame are very desirable. To address this demand, we are developing a new numerical tool based on *OpenFOAM* [1] which can be utilized to simulate the free-surface dynamics of the melt flow under the influence of alternating electromagnetic fields. The underlying multi-physical model involves three-dimensional hydrodynamic and magnetodynamic effects and their interaction.

Keywords: Ribbon Growth on Substrate, numerical simulation, coupled multi-physics, free-surface flow, eddy-currents

1. Introduction

The central idea of the RGS process [2, 3] is a continuous feeding of molten semi-conductor material into a bottomless casting frame, while a solidified foil (ribbon) is extracted sidewise on a sub-cooled moving substrate underneath. Fig. 1 depicts the main parts and outlines the process principle. Excitation coils, which are necessary for inductive heating, bear a two-fold meaning. The generated AC magnetic field is designed to provide both heat and a kind of magnetic valve. The latter actively prevents leakage of melt from the slit region between casting frame and substrate and reduces flow-oscillations at the extraction site of the silicon foil through electromagnetic forces. That is, magnetic forces act to counter the gravitational forces on the melt, supporting the effect of surface tension on the free-surface in the slit region.

2. Numerical Model

In the real RGS process [2], the casting region is a complex and detailed system. Many parts of this system have only limited influence on the melt flow. In order to reduce computational efforts, a simplified set of modeling parameters and casting environment geometry was derived for our numerical approach. For this model the RGS wafer size is given by $156\,mm \times 156\,mm \times 0.5\,mm$. The mean melt level height inside the casting frame is assumed to be $h = 20\,mm$, the length of the melt region in process direction is $l = 70\,mm$ and the width $w = 150\,mm$. A typical set of process parameters is a RMS-current of $I_{RMS} = 1000$ A at a frequency of $f = 10$ kHz to feed the excitation coils in combination with

* Corresponding author: Pascal Beckstein, Department of Magnetohydrodynamics, Institute of Fluid Dynamics, Helmholtz-Zentrum Dresden-Rossendorf, Bautzner Landstraße 400, D-01328 Dresden, Germany, Tel.: +49 351 260 3119; Fax +49 351 260 2007; E-mail: p.beckstein@hzdr.de.

a substrate velocity of $u_S = 0.1\ \mathrm{m/s}$ in process direction. The most important properties of the materials shown in Fig. 1 are listed in Table 1.

Considering the assembly of all conducting parts inside and around the excitation coil (cf. Fig. 1) as one non-magnetizable, conducting domain Ω_C with locally varying conductivity, the physical description of the magnetic fields can be regarded as a typical eddy current problem [4] according to the scheme in Fig. 2. The skin depths δ as specified in Table 1 denote the characteristic penetration depths of the alternating magnetic flux into each material. Our mathematical formulation is based on the so called $\boldsymbol{A}$,V-$\boldsymbol{A}$-formulation [4, 5] for small magnetic Reynolds numbers $R_m = \mu_0 \sigma U L \ll 1$ [6]. This is valid for our purposes taking into account a typical reference velocity of $U = 1\ m/s$ and the mean melt height as reference length $L = h$ in combination with the properties of the melt from Table 1. Given the velocity field $\boldsymbol{u}$ and the physical time t, we may introduce the magnetic vector potential $\boldsymbol{A}$ with applied Coulomb-Gauge and the electric scalar potential V in Ω_C as follows:

$$\boldsymbol{B} = \boldsymbol{\nabla} \times \boldsymbol{A}\ ; \quad \boldsymbol{\nabla} \cdot \boldsymbol{A} = 0\ ; \tag{1}$$

$$\boldsymbol{E} = -(\partial_t \boldsymbol{A} + \boldsymbol{\nabla} V)\ ; \quad \|\boldsymbol{u} \times \boldsymbol{B}\| / \|\boldsymbol{E}\| \ll 1\ . \tag{2}$$

The quasi-static Maxwell-Equations with MHD approximation [4, 6] for the conducting domain Ω_C then becomes

$$\boldsymbol{\nabla} \times \boldsymbol{\nabla} \times \boldsymbol{A} + \sigma \mu_0 (\partial_t \boldsymbol{A} + \boldsymbol{\nabla} V) = \boldsymbol{0}\ , \tag{3}$$

with the solely induced current density according to Ohm's law - the eddy currents:

$$\boldsymbol{j} = -\sigma (\partial_t \boldsymbol{A} + \boldsymbol{\nabla} V)\ . \tag{4}$$

An additional equation for V can be derived from (4) to satisfy current conservation ($\boldsymbol{\nabla} \cdot \boldsymbol{j} = 0$) in Ω_C in the case of a three-dimensional domain:

$$\boldsymbol{\nabla} \cdot (\sigma \boldsymbol{\nabla} V) = -\boldsymbol{\nabla} \cdot (\sigma \partial_t \boldsymbol{A})\ . \tag{5}$$

To allow for discontinuities in σ, we have developed specialized interpolation and discretization schemes, which are strictly current conserving.

Maxwell's equations [4] are actually defined on an unbounded domain. To capture this numerically, the conducting region itself is being surrounded by a non-conducting region Ω_0 ($\sigma \equiv 0$) which extends up to a sufficiently large distance from the interface $\Gamma_C = \Omega_C \cap \Omega_0$ between both domains and from the location of the excitation coil (cf. Fig. 2). The size of the non-conducting region can be determined empirically. Starting from a first selection, its size can be increased successively until the magnetic field inside the conductor does not change significantly anymore.

Using the definition of $\boldsymbol{A}$ and V to substitute the magnetic field $\boldsymbol{B}$ and the electric field $\boldsymbol{E}$, enables us to explicitly introduce an external source current density $\boldsymbol{j}_0$ (claiming $\boldsymbol{\nabla} \cdot \boldsymbol{j}_0 = 0$) in the governing equations for Ω_0 to model the inductor. If this is elaborated, $\boldsymbol{A}$ needs to hold

$$\boldsymbol{\nabla} \times \boldsymbol{\nabla} \times \boldsymbol{A} = \mu_0 \boldsymbol{j}_0 \tag{6}$$

in the non-conducting region.

The outer boundary Γ_∞ of Ω_0 with its normal $\boldsymbol{n}_\infty$ is modelled as tangentially magnetic. A corresponding boundary condition for the Coulomb gauged magnetic vector potential $\boldsymbol{A}$ can be identified from this as:

$$\boldsymbol{A} \times \boldsymbol{n}_\infty = 0\,; \quad \partial_{\boldsymbol{n}_\infty} \boldsymbol{A} \cdot \boldsymbol{n}_\infty = 0\,. \tag{7}$$

It is worth to note that using equation (7) will not truncate the magnetic field $\boldsymbol{B}$ on Γ_∞. It rather forces the magnetic field lines to be closed within the non-conducting region as if the numerical model would be in a magnetically insulating box. A more strict modelling of this far-field boundary would be to use a purely homogeneous Dirichlet boundary condition.

Across the conductor interface Γ_C, the Coulomb gauged magnetic vector potential $\boldsymbol{A}$ remains continuous. The current density $\boldsymbol{j}$ needs to vanish in normal direction $\boldsymbol{n}_\mathrm{C}$. To fulfill this requirement, it is necessary to apply an inhomogeneous Neumann-boundary condition for V, which represents a charge accumulation in order to counter the rate of change of the magnetic field:

$$\boldsymbol{\nabla} V \cdot \boldsymbol{n}_C = \partial_t \boldsymbol{A} \cdot \boldsymbol{n}_C\,. \tag{8}$$

The $\boldsymbol{A}$,V-$\boldsymbol{A}$-formulation as given above can be transformed into a quasi-stationary formulation. Thereby complex-valued sinusoidal fields for an angular frequency of $\omega = 2\pi f$ are introduced. This is valid since the excitation coil in the real RGS process is part of an oscillation circuit and thus driven by a sinusoidally alternating current with resonance frequency. After switching to the complex domain, it is possible to replace all time derivatives of $\boldsymbol{A}$ with a complex-valued angular frequency ($\partial_t = i\omega$).

As already mentioned in the introduction, a new algorithm for the numerical solution of the magnetodynamic system has been developed on the basis of the *OpenFOAM Extend Project* (www.extend-project.de). The novel solver-implementation called *eddyCurrentFoam* uses a partially coupled approach to deal with the challenging $\boldsymbol{A}$,V-system. For the complex parts of $\boldsymbol{A}$ in the frequency domain, the component-wise coupling is directly integrated into the finite-volume discretization process on the whole region Ω. A segregated coupling is then used to link $\boldsymbol{A}$ and V together, where the electric scalar potential is only solved on Ω_C. The implementation of our new *eddyCurrentFoam*-solver has already been validated. A detailed description of its concept would however go beyond the scope of this paper. More details and a comparison of results for an appropriate test case with a commercial finite-element software will be published elsewhere.

The fluid dynamics of the melt (cf. Fig. 1) is governed by the principle of conservation of mass and momentum in form of the Navier-Stokes-Equation [7]. The melt is modelled as an incompressible, isothermal Newtonian fluid. Eddy currents $\boldsymbol{j}$ from (4) and the magnetic field $\boldsymbol{B}$ corresponding to (1) have an effect on the momentum balance via the time-averaged Lorentz force

$$\boldsymbol{F}_L = \langle \boldsymbol{j} \times \boldsymbol{B} \rangle_t\,. \tag{9}$$

Following Ampere's law, $\boldsymbol{F}_\mathrm{L}$ can be expressed as a sum of its rotational and gradient part

$$\boldsymbol{F}_L = 1/\mu_0 \langle (\boldsymbol{B} \cdot \boldsymbol{\nabla}) \boldsymbol{B} \rangle_t - \boldsymbol{\nabla} p_B, \tag{10}$$

where p_B is the time-averaged magnetic pressure given by

$$p_\mathrm{B} = 1/(2\mu_0) \langle \boldsymbol{B^2} \rangle_t \,. \tag{11}$$

Besides magnetic forces, gravitational forces are acting on the fluid such that the above can be concluded to

$$\rho[\partial_t \boldsymbol{u} + (\boldsymbol{u} \cdot \boldsymbol{\nabla}) \boldsymbol{u}] = \boldsymbol{\nabla} \cdot \boldsymbol{\tau}' + 1/\mu_0 \langle (\boldsymbol{B} \cdot \boldsymbol{\nabla}) \boldsymbol{B} \rangle_t \,; \quad \boldsymbol{\nabla} \cdot \boldsymbol{u} = 0 \,, \tag{12}$$

where the stress tensor

$$\boldsymbol{\tau}' = \eta[\boldsymbol{\nabla u} + (\boldsymbol{\nabla u})^T] - p' \boldsymbol{I} \tag{13}$$

is based on a modified diagonal fluid pressure including magnetic and gravitational pressure:

$$p' = p + p_G + p_B \quad with \quad p_G = -\rho(\boldsymbol{g} \cdot \boldsymbol{x}) \,. \tag{14}$$

In the equations above, the fluid density is denoted with ρ, the dynamic viscosity of the fluid with η, the physical pressure with p and $\boldsymbol{x}$ is the field of position vectors. Currently solidification and thermal energy transport is not modelled, but an extension is possible at a later stage of development.

The fluid domain is bounded by the top free-surface, side walls (casting frame) and the liquid/solid interface at the bottom (substrate). The latter is assumed to be planar and being translated with the horizontal casting velocity $\boldsymbol{u}_\mathrm{S}$ of the moving substrate. The free-surface boundary Γ_F with $\Gamma_\mathrm{F} \in \Gamma_\mathrm{C}$ is influenced by strong surface tension. The viscosity of the external atmosphere, which is in contact with the liquid melt at the free-surface, is several orders of magnitude smaller than the viscosity of the melt itself. In this regard, the fluid boundary condition at the free-surface with its velocity $\boldsymbol{u}_\mathrm{F}$, unit normal field $\boldsymbol{n}_\mathrm{F}$, unit tangent field $\boldsymbol{t}_\mathrm{F}$ and the stress vector $\boldsymbol{s}_\mathrm{F} = \boldsymbol{\tau}' \cdot \boldsymbol{n}_\mathrm{F}$ is modeled as simplified Young-Laplace-Equation [8]

$$\boldsymbol{s}_F \cdot \boldsymbol{n}_F = 2\kappa\gamma - (p_B + p_G) \,; \quad \boldsymbol{s}_F \cdot \boldsymbol{t}_F = 0 \,; \tag{15}$$

$$\kappa = -1/2 \cdot (\boldsymbol{\nabla}_\Gamma \cdot \boldsymbol{n}) \,; \quad \boldsymbol{\nabla}_\Gamma = \boldsymbol{\nabla} - \boldsymbol{n}\partial_{\boldsymbol{n}} = (\boldsymbol{I} - \boldsymbol{n}\boldsymbol{n}^T)\boldsymbol{\nabla} \tag{16}$$

with

$$\boldsymbol{u} \cdot \boldsymbol{n}_F = \boldsymbol{u}_F \cdot \boldsymbol{n}_F \,. \tag{17}$$

The surface gradient operator $\boldsymbol{\nabla}_\Gamma$ from equation (16) defines the mean curvature κ of the free-surface and γ represents the constant surface-tension coefficient. Stationary walls are modelled with no-slip boundary conditions, whereas for the bottom wall of the fluid domain an inhomogeneous Dirichlet boundary condition is applied to simulate the substrate movement.

The flow calculation and the dependent free-surface movement is modelled and solved within the same three-dimensional finite-volume method as the electromagnetic part. Similar to the solution of $\boldsymbol{A}$ and V, the solution of $\boldsymbol{u}$ and p' from equation (12) and (13) is determined

in a segregated manner according to the so called PISO-algorithm [7] for given Lorentz force and magnetic pressure. A surface tracking method with a dynamic moving mesh [8, 9] based on an extended version of the *interTrackFoam* solver algorithm [10] is used to adjust the interface in order to achieve a vanishing normal flux at the free-surface. According to equations (15) to (17) and the current shape of the top free-surface, a variable Dirichlet boundary for p' and an inhomogeneous Neumann boundary condition for $\boldsymbol{u}$ can be formulated on Γ_F. These boundary conditions are iteratively re-calculated and coupled to the flow variables for each time step until the free-surface flux is negligibly small and all initial residuals are below predefined thresholds. Typically five to ten iterations are necessary to achieve a reasonable small error.

The underlying concept of the whole surface tracking method is based on the Arbitrary Lagrangian-Eulerian formulation (ALE). This formulation is used to account for the mesh movement. The mesh moves independently from the fluid flow, except for the domain boundaries. For our model, the free-surface is under constraint, such that the fluid velocity equals the mesh velocity $\boldsymbol{u}_\mathrm{M}$ in normal direction. For all other boundaries, $\boldsymbol{u}_\mathrm{M}$ is restricted according to the meaning of the boundary for the mesh (e.g. slip/no-slip). The independent mesh-movement away from the boundaries allows a free and preferably smooth mesh point distribution. In our case a Laplace-smoothing for $\boldsymbol{u}_\mathrm{M}$ was utilized [11]. The inner mesh is however only adjusted and smoothed once per time step and not within the free-surface adjustment iterations. In the sense of ALE, the governing equation (12) of the hydrodynamic problem needs to be considered as relative to the mesh motion $\boldsymbol{u}_\mathrm{M}$ in a Lagrangian manner. The mesh movement is incorporated by means of replacing the time-derivative in (12) with the material derivative. This introduces an additional convection term, such that we obtain:

$$\rho[D_t\boldsymbol{u} + (\boldsymbol{u}\cdot\boldsymbol{\nabla})\boldsymbol{u} - (\boldsymbol{u}_M\cdot\boldsymbol{\nabla})\boldsymbol{u}] = \boldsymbol{\nabla}\cdot\boldsymbol{\tau}' + 1/\mu_0\langle(\boldsymbol{B}\cdot\boldsymbol{\nabla})\boldsymbol{B}\rangle_t\,; \quad \boldsymbol{\nabla}\cdot\boldsymbol{u} = 0\,. \tag{18}$$

In *OpenFOAM*, the second convection term is implicitly treated on the basis of the so called mesh flux, which is derived from the current mesh velocity. As the convection term is already linearized and discretized with the flux of the fluid velocity, subtracting the flux of the mesh velocity from the former is sufficient for a description of (12) in a relative reference system. Further details about the surface tracking method can be found in [10].

Since the spatial distribution of the electrical conductivity inside the whole numerical domain $\Omega = \Omega_\mathrm{C} \cup \Omega_0$, as shown in Fig. 2, depends on the current location of the free-surface Γ_F, it is obvious that there is a two-fold coupling mechanism between the magnetodynamic equations (3), (5), (6) and the hydrodynamic equation (12) due to the Lorentz force (10) and $\sigma = \sigma\big(\boldsymbol{x}(\boldsymbol{u}_\mathrm{M})\big)$. Compared to one time-step of the hydrodynamic part, the numerical solution of the magnetodynamic problem is computationally very expensive especially in three dimensions. In general, the system of equations (3), (5) and (6) in their complex form is equivalent to a system of eight strongly coupled scalar-valued Poisson-type equations. The surface-tracking approach now allows to "carry" the Lorentz force distribution $\boldsymbol{F}_\mathrm{L}\big(\boldsymbol{x}(\boldsymbol{u}_\mathrm{M})\big)$ with the mesh for a defined and reasonable small simulation time. This reduces the computational effort to solve the whole coupled system.

To combine the solution of $\boldsymbol{A}, V$ and $\boldsymbol{u}$, p' in the same framework we have developed a new multi-mesh backend in *OpenFOAM Extend Project* based on several superposed meshes for fast and direct, bi-directional mapping. On the one hand, Lorentz force and magnetic

pressure are calculated from $\boldsymbol{A}$ and V in the conducting domain Ω_C. They are consequently mapped to the fluid domain Ω_F prior to the flow calculation. On the other hand, before the magnetic field calculation is repeated during the simulation, the mesh of the conducting and the background region is adjusted to the current shape of the fluid domain. The multi-mesh backend, *eddyCurrentFoam* and our extended *interTrackFoam* were combined to one multi-physics software tool called *interTrackEddyCurrentFoam*, where no interpolation of bulk data is necessary to couple the magnetodynamic and hydrodynamic fields. This is a major advantage compared to similar techniques [12, 13], whose different numerical methods like finite-volume and finite-element are combined via interpolation and periodically re-generated meshes. More details concerning the whole numerical method will be published separately.

3. Simulation results

In previous studies [14] we have provided an overview of the magnetohydrodynamic effects in the RGS process at its characteristic process parameters as given above. We have already performed 3D-simulations with fixed melt geometry to numerically confirm the functioning melt retention based on magnetic fields. Analyzing the corresponding data, it has been illustrated that the retention effect is correlated with a strong forced fluid flow with velocities up to $U = 1\,m/s$. That is, the influence of the Lorentz force on the fluid flow is much more intense than the drag force from the moving substrate wall. In particular, we also demonstrated that the surface deformation is substantially influencing global flow patterns such as the typical size of the vortices close the side walls. The Lorentz force acting on a conducting liquid inside a coil is roughly pointing towards the center of this coil. Consequently, the shape of the deformed fluid domain for these and similar cases looks like a dome. This typical kind of deformation is therefore often referred to as "dome-shaping" [6]. We demonstrated the numerical simulation of this dome-shaping effect for the RGS process by means of a two-dimensional model in [15], where we used *COMSOL Multiphysics* [16] as tool for the magnetodynamic part of the simulation. It turned out that the combination of *OpenFOAM* and *COMSOL Multiphysics* is not suitable for large 3D-simulations due to several reasons. The central issue with this external coupling of fundamentally different software tools, even if all steps were already fully automated, is the overhead produced by interpolation, mesh generation and free-surface extraction. With our new method as explained in the last section we overcame these obstacles completely. The following results still have to be considered more as demonstration of this novel method, rather than a validation case. Basic testing of the new *interTrackEddyCurrentFoam*-solver is already completed, but a comprehensive validation is yet to follow.

As a new proof of concept, Fig. 3 (process direction is always from left to right) shows a time-series of the free-surface flow inside the fluid domain with its evolving dome-shape for a three-dimensional model of the RGS process according to Fig. 1. The underlying numerical mesh comprises a total of $\approx 1.5 \times 10^6$ cells (background: 8.8×10^5, fluid: 1.5×10^5, other conducting parts: 4.7×10^5). A simulation time of ten seconds took approximately one week of calculation time on one single core of a modern CPU with a dynamic time step width based on an average value of $\Delta t_\mathrm{mean} = 2.0 \times 10^{-4} s$. The Lorentz force was updated periodically with a time step width of $\Delta t_{\boldsymbol{F}_\mathrm{L}} = 0.01\,s$. A direct comparison of the computational performance with similar models of other authors (e.g. [13]) is very difficult as the available information is very limited. In [13] it is stated in section 4.3 that the calculation of ten seconds simulation time took three months on four CPUs in parallel. This is approximately 24 times

more than the necessary computational time for our three-dimensional RGS-model. Any information about the mesh size of the corresponding model in section 4.3 of [13] is however missing. Although it might be similar to the size of our RGS model, as the geometrical dimensions are roughly in the same order of magnitude, some uncertainty remains.

To allow unsteady RANS-simulations on coarser meshes, the usage of turbulence and sub-grid-scale-models of *OpenFOAM* has been implemented in our solver, too. The k-ω-SST turbulence model [17] was used in our case. At the start of the simulation ($t = 0\ s$), the magnetic field was applied for a constant surface level of $h = 20\ mm$. In the left column of Fig. 3 one can comprehend how the three-dimensional dome-shape is evolving during time. Here, the front contour of the fluid region shows the magnitude of the velocity field ($\|\boldsymbol{u}\|\ [m/s]$), and the back contour indicates the time-averaged Lorentz force density ($\boldsymbol{F}_\mathrm{L}/\rho[m/s^2]$). In the middle column of Fig. 3, the development of the flow velocity at a central section in process direction is presented. The right column finally illustrates how the velocity field changes during time at a central horizontal section at a height of $h = 10\ mm$.

During the first second, there is evidently a good agreement with the results of our 2D-case [15] regarding to velocity magnitude and flow structure. At later times, three-dimensional effects eventually get more and more dominant. After approximately 4-5 seconds, two large vortices begin to emerge from four smaller ones. Those two large eddies seem to be quasi-stable, as they persist even for long runs with $t > 10\ s$.

4. Conclusion

The RGS process [2, 3] is a promising technology for the production of silicon wafers and advanced metal-silicide alloys. Detailed insights from modelling the characteristic melt flow in the casting frame are very desirable. There are many related industrial applications, where the analysis of similar magnetohydrodynamic effects is of great interest. Within this paper we have introduced a novel numerical method and corresponding software for the simulation of the free-surface dynamics of conducting fluids under the influence of magnetic fields. This tool is based on the framework of the *OpenFOAM Extend Project*. From a global analysis of the RGS process [14] and comprehensive tests we revised our previous approach [15] and combined a new eddy current solver and an extended surface tracking method within the same multi-mesh finite-volume method. The realization now allows us to perform three-dimensional simulations of the RGS process and similar problems at minimal computational costs. A proof of concept was made and first test cases revealed satisfying three-dimensional results compared to well-established tools like *COMSOL Multiphysics*. There are still remaining problems concerning numerical stability and dynamic mesh handling as our method relies on some cutting-edge developments of *OpenFOAM Extend Project*. These issues are subject of current and future investigation. To validate our newly developed code, future work will also be devoted to prepare experimental test cases for comparison.

Acknowledgements

Financial support for this research from the German Helmholtz Association in frame of the Alliance “Liquid Metal Technologies (LIMTECH)” is gratefully acknowledged.

References

[1] H. Weller, G. Tabor, H. Jasak and C. Fureby, A tensorial approach to computational continuum mechanics using object oriented techniques, *Computational Physics*, vol. **12**(6) (1998), no. 6, 620-631.

[2] A. Schönecker, L. J. Geerligs and A. Müller, Casting Technologies for Solar Silicon Wafers: Block Casting and Ribbon-Growth-on Substrate, *Solid State Phenomena*, Vols. **95-96** (2004), 149-158.

[3] G. Hahn and A. Schönecker, New crystalline silicon ribbon materials for photovoltaics, *Journal of Physics: Condensed Matter*, **16** (2004), R1615-R1648.

[4] K. J. Binns, P. J. Lawrenson and C. W. Trowbridge, The Analytical and Numerical Solution of Electric and Magnetic Fields, Wiley, 1992.

[5] O. Biro and A. Valli, The Coulomb gauged vector potential formulation for the eddy-current problem in general geometry: Well-posedness and numerical approximation, *Computer Methods in Applied Mechanics and Engineering*, **196** (2007), 1890-1904.

[6] R. Moreau, Magnetohydrodynamics, Kluwer, 1990.

[7] J. H. Ferziger and M. Peric, Computational Methods for Fluid Dynamics, Springer-Verlag, 2002.

[8] R. Scardovell and S. Zalesk, Direct Numerical Simulation of Free Surface and Interfacial Flow, *Annual Review of Fluid Mechanics*, **31** (1999), 567-603.

[9] H. Jasak, Dynamic Mesh Handling in OpenFOAM, in *47th AIAA Aerospace Sciences Meeting Including The New Horizons Forum and Aerospace Exposition*, Orlando, 2009.

[10] Z. Tukovic and H. Jasak, A moving mesh finite volume interface tracking method for surface tension dominated interfacial fluid flow, *Computers & Fluids*, **55** (2012), 70-84.

[11] H. Jasak and Z. Tukovic, Automatic mesh motion for the unstructured finite volume method, *Transactions of FAMENA*, **30**(2) (2007), 1-18.

[12] S. Spitans, A. Jakovics, E. Baake and B. Nacke, Numerical Modeling of Free Surface Dynamics of Melt in an Alternate Electromagnetic Field: Part I. Implementation and Verification of Model, *Metallurgical and Materials Transactions B*, **44**(3) (2013), 593-605.

[13] S. Spitans, E. Baake, B. Nacke and A. Jakovics, A numerical model for coupled free surface and liquid metal flow calculation in electromagnetic field, *International Journal of Applied Electromagnetics and Mechanics*, **44** (2014), 171-182.

[14] P. Beckstein, V. Galindo and G. Gerbeth, Electromagnetic flow control in the Ribbon Growth on Substrate (RGS) process, *Magnetohydrodynamics*, **51** (2015), 385-396.

[15] P. Beckstein, V. Galindo and G. Gerbeth, Free-surface dynamics in the Ribbon Growth on Substrate (RGS) process, *Proceedings of the 8th International Conference on Electromagnetic Processing of Materials*, 167-170, 2015.

[16] *COMSOL 5.1 Multiphysics Reference Manual*, 2015.

[17] F. R. Menter, Two-equation eddy-viscosity turbulence models for engineering applications, *AIAA Journal*, **32**(8) (1994), 1598-1605.

[18] S. Spitans, E. Baake, B. Nacke and A. Jakovics, Numerical Modeling of Free Surface Dynamics of Melt in an Alternate Electromagnetic Field: Part II. Conventional Electromagnetic Levitation, *Metallurgical and Materials Transactions B*, **47**(1) (2015), 522-536.

Material	ρ [kg/m^3]	η [Pa · s]	σ [S/m]	γ [N/m]	δ [mm]
Liquid silicon (melt)	2580	0.86×10^{-3}	1.20×10^{6}	0.733	5.0
Solid silicon (melt/wafer)	2330	-	8.30×10^{4}	-	17.0
Graphite (casting frame)	1880	-	1.25×10^{5}	-	14.0
Copper (inductor)	8960	-	6.00×10^{7}	-	0.7

Table 1: Properties for different materials: Density ρ, dynamic viscosity η, electrical conductivity σ, surface tension γ for contact with air and skin depth $\delta = \sqrt{1/(\pi f \mu_0 \sigma)}$ for a frequency of $f = 10\ kHz$.

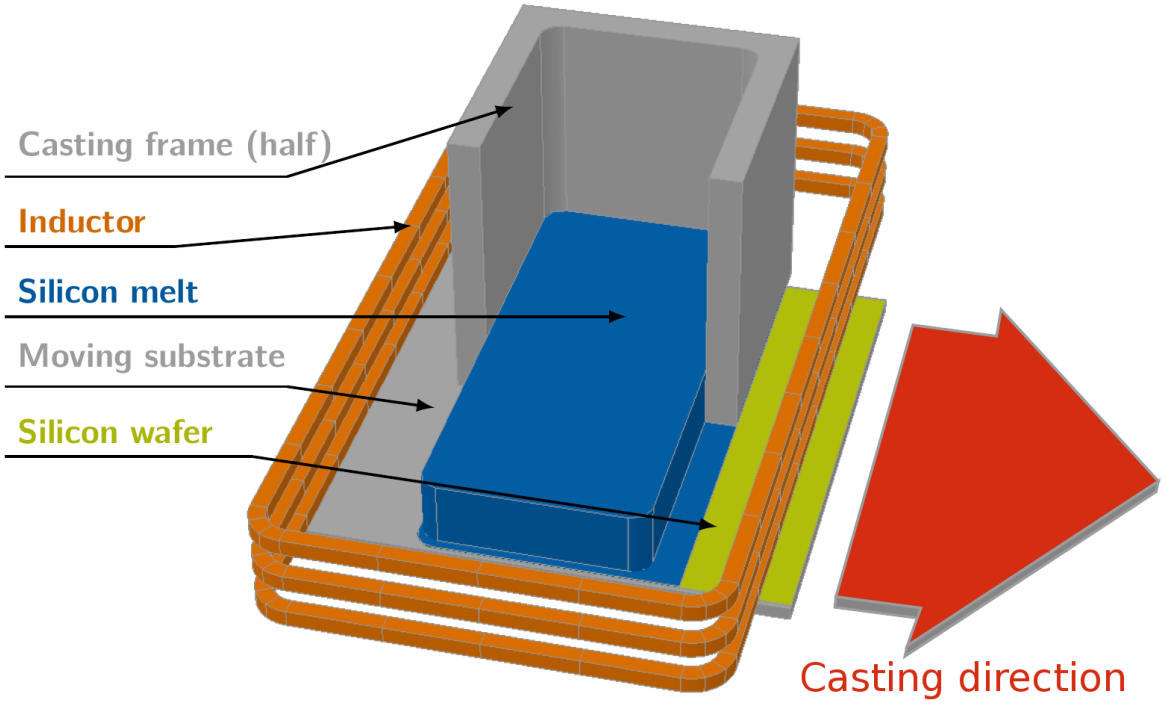

Fig. 1: Scheme of the RGS process with silicon [2].

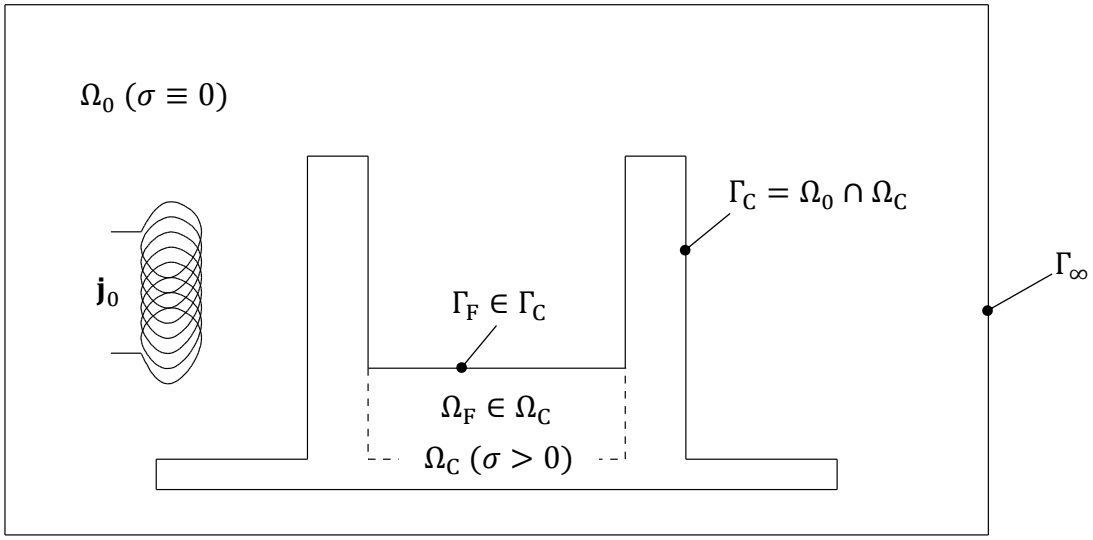

Fig. 2: Domain decomposition with non-conducting region Ω_0 and conducting region Ω_C with its fluid sub-region Ω_F (dashed line). The free-surface Γ_F of the fluid is part of the conductor surface Γ_C. The excitation coil is modelled as source current density $\mathbf{j}_0$.

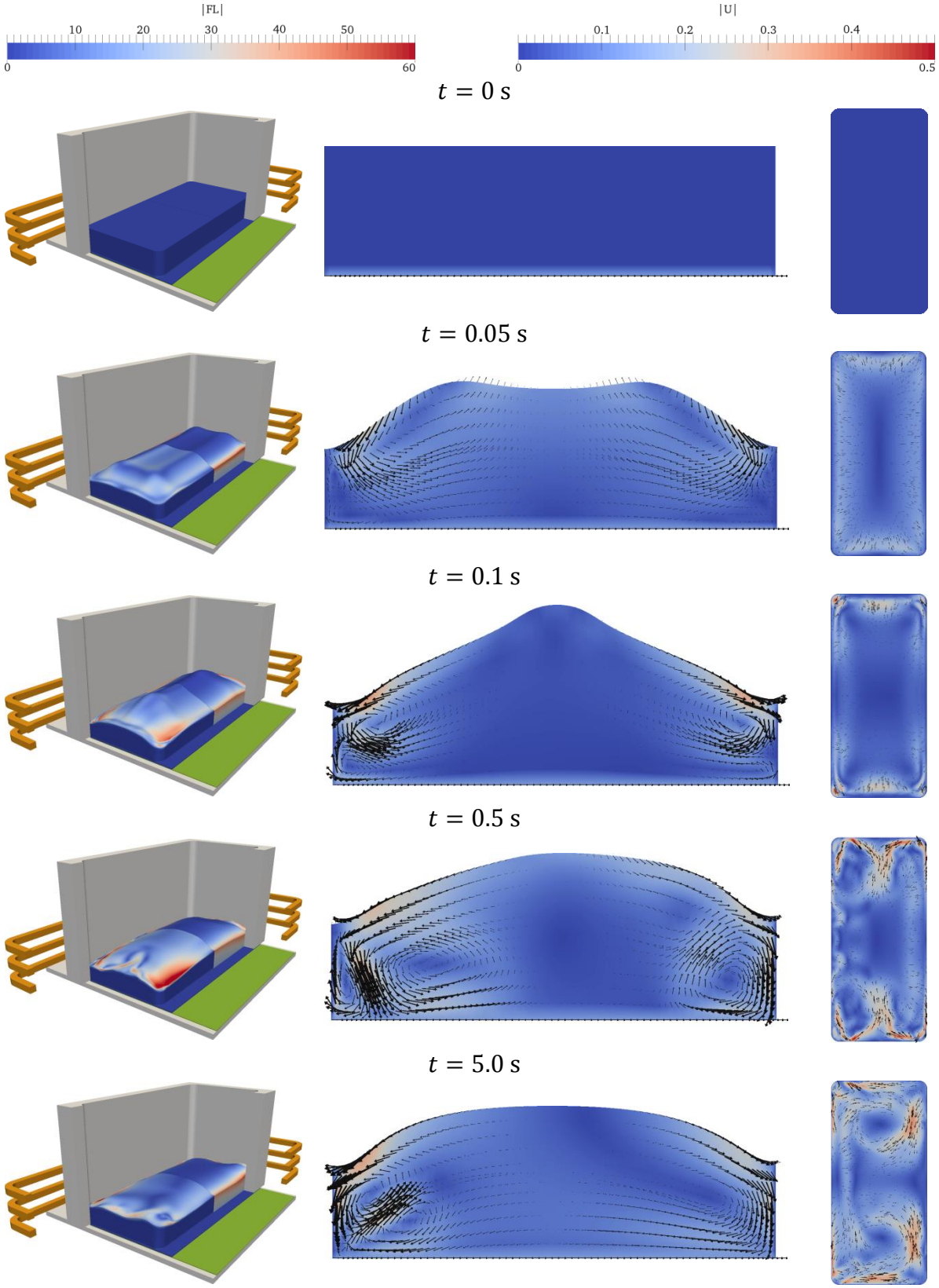

Fig. 3: Evolution of the 3D free-surface flow after applying the magnetic field for a constant surface level at $t = 0\ s$ (left column, front contour: $\|\boldsymbol{u}\|\ [m/s]$, back contour: $\boldsymbol{F}_{\mathrm{L}}/\rho[m/s^2]$): Velocity field vectors and contour at the central section in process direction (middle column) and at a central horizontal section (right column) of the fluid domain. The Lorentz force was updated every $\Delta t_{\boldsymbol{F}_{\mathrm{L}}} = 0.01\ s$. (Process direction is from left to right)